Physics of Plasmas

Observation of spontaneous decay of Alfvénic fluctuations into co- and counter-propagating magnetosonic waves in a laboratory plasma

Cite as: Phys. Plasmas **26**, 032105 (2019); https://doi.org/10.1063/1.5082802
Submitted: 24 November 2018 . Accepted: 22 February 2019 . Published Online: 14 March 2019

Peiyun Shi, Zhida Yang, Ming Luo, Rongsheng Wang, Quanming Lu, and Xuan Sun

Observation of spontaneous decay of Alfvénic fluctuations into co- and counter-propagating magnetosonic waves in a laboratory plasma

Cite as: Phys. Plasmas **26**, 032105 (2019); doi: 10.1063/1.5082802
Submitted: 24 November 2018 · Accepted: 22 February 2019 ·
Published Online: 14 March 2019

View Online Export Citation CrossMark

Peiyun Shi,[1] Zhida Yang,[1] Ming Luo,[1] Rongsheng Wang,[2] Quanming Lu,[2] and Xuan Sun[1,a)]

AFFILIATIONS

[1]Department of Engineering and Applied Physics, University of Science and Technology of China, Hefei 230026, China
[2]Department of Geophysics and Planetary Science, University of Science and Technology of China, Hefei 230026, China

[a)]Email: xsun@ustc.edu.cn

ABSTRACT

We show experimentally that Alfvénic fluctuations can spontaneously decay into a fast and a slow magnetosonic wave in an inhomogeneous plasma. The fast wave of higher frequency propagates in the same direction, while the slow wave of lower frequency propagates in the opposite direction with the pump wave. Both of the daughter waves are characterized by strong parallel but modest perpendicular fluctuations. The measured frequencies and wavenumbers are found to satisfy the energy and momentum conservation conditions for a nonlinear three wave interaction. The evidence of energy flowing from pump fluctuations into daughter waves is also presented in this paper. The results may shed light on the origin of inward Alfvén waves observed in the solar corona and chromosphere and how shear Alfvén waves deposit its energy by driving compressional perturbations.

I. INTRODUCTION

The laboratory simulation of space plasma has continuously enriched our understanding of plasma behavior in the planetary and stellar atmosphere, for example, magnetic reconnection, wave-particle interaction, and magneto-rotational instability.[1–4] As the most fundamental wave mode in magnetized plasmas, Alfvén waves could also play a role in the heating and evolution of space, astrophysical, and laboratory plasmas.[5] Many experiments have been thus devoted to the study of Alfvén waves and revealed many faces of Alfvén waves.[6–9]

Due to their incompressible nature, shear Alfvén waves (SAWs) have been considered as the primary carrier of energy to the coronal region; on the other hand, there must exist a mechanism(s) to convert their energy into heat which accounts for the mysterious high temperature of the corona. The conversion does not need to be very efficient as a small amount ($\sim$0.1%) of output energy from the interior is enough to heat up the tenuous corona.[10] Of various hypotheses, two candidates are of particular interest here: (1) parametric excitation of ion sound waves[11,12] or other compressional waves[13] and (2) turbulent heating from a nonlinear cascade of multiple wave interactions.[14–16] Although related theoretical and numerical investigations[17,18] of space plasma have been conducted extensively, few laboratory observations of simulating plasmas have been reported. By deliberately launching two Alfvén waves at different frequencies, ion sound waves with differential frequency were successfully launched through beating of these two waves in Large Plasma Devices (LAPDs).[19,20] Recently, Dorfman *et al.*[21] observed that a kinetic Alfvén wave can produce two sidebands of Alfvén waves and a low frequency non-resonant mode due to modulational instability. We will show in this paper that shear Alfvénic fluctuations (SAFs) could also spontaneously decay into co- and counter-propagating magnetosonic waves in a laboratory plasma, and the decay channel is robust. Note that this process has been considered in theories;[13,22–25] however, this kind of decay channel has not been observed in a laboratory plasma, to the authors' knowledge.

The turbulent cascade of non-compressional waves requires a counter-propagating wave.[15,26] Although the magnetic structures in solar plasmas have been frequently inspected by satellite imaging and spectroscopic systems, the identification of the wave's direction has posed challenges. Recently, Mortan *et al.*[27] reported the observation of inward Alfvén waves in the coronal region and Liu *et al.*[28] found the counter-propagating compressive fluctuation in the chromosphere. Notably, an inward propagating wave can be generated by the wave reflection or parametric decay, while in this paper, we show that counter-propagating (inward) magnetic waves can be produced by the latter process.

The rest of this paper is arranged as follows: Sec. II introduces the experimental setup including the SAF launching antenna and diagnostic tools. The energy and momentum conservation constrains are shown to be satisfied in Sec. III to validate the three wave interaction during this spontaneous decay process of SAFs. The identification of daughter wave modes is also provided in this section. Section IV shows the evidence of the energy transferring process. Finally, Sec. V presents a brief discussion and the conclusion of this paper.

II. EXPERIMENTAL SETUP

The experiments were conducted using a 10-m long tandem mirror device, KMAX (Keda Mirror with AXisymmetricity), which consists of one central cell and two end cells.[29] Their dimensions are shown in Fig. 1(a), and the green dashed lines represent the DC magnetic field, pointing toward $+z$, which is typically 275 gauss in the central cell and 1900 gauss at the mirror throat. In this work, the plasma is produced by a helicon antenna located at the right end, $z \sim 5.05$ m, the RF power is typically 2 kW with frequency at 13.56 MHz, and the gas species is hydrogen. Helicon plasmas have been widely used in space plasma simulation due to their easy operation and high ionization rate.[30] In our application, the source plasma expands into downstream by following the background magnetic field lines. The key to the experiments reported here is to form a plasma column through the entire device, i.e., a 10 m long plasma column. Typical plasma parameters are $n_e \sim (1-4) \times 10^{16}\,\mathrm{m}^{-3}$ and $T_e \sim 4-10$ eV. Radial density profiles measured by four triple Langmuir probes PE1–4 at four different axial positions are given in Fig. 1(b). The SAF is launched by a solenoidal antenna at $z = 1.00$ m and $r = 0.05$ m. A nominal 7 kW oscillator at a frequency of $f = 368$ kHz or $\omega \sim 0.89\,\Omega_{ci}$, where Ω_{ci} is the ion cyclotron frequency, feeds current into the antenna via an isolation transformer. The antenna current measured using a Pearson Current Monitor is $\sim$100 A, which can produce the magnetic field B_x of $\sim$20 gauss, 7.3% of the background magnetic field strength. Four sets of electrically shielded magnetic probes PBE1, PBE2, PBW1, and PBW2 are placed at $z = 0.00$ m, 0.50 m, 1.67 m, and 3.25 m, respectively, to detect magnetic fluctuation. PBW1 also integrates a single electric probe at the top to measure the ion saturation currents. All signals from probes are connected to oscilloscopes with a sampling rate at 5 MS/s.

III. OVERVIEW OF THE SPONTANEOUS DECAY PHENOMENON

A. Energy conservation

For any nonlinear three wave interaction, energy and momentum have to be conserved: $f = f_1 + f_2$ and $\mathrm{k} = \mathrm{k}_1 + \mathrm{k}_2$. These conservation

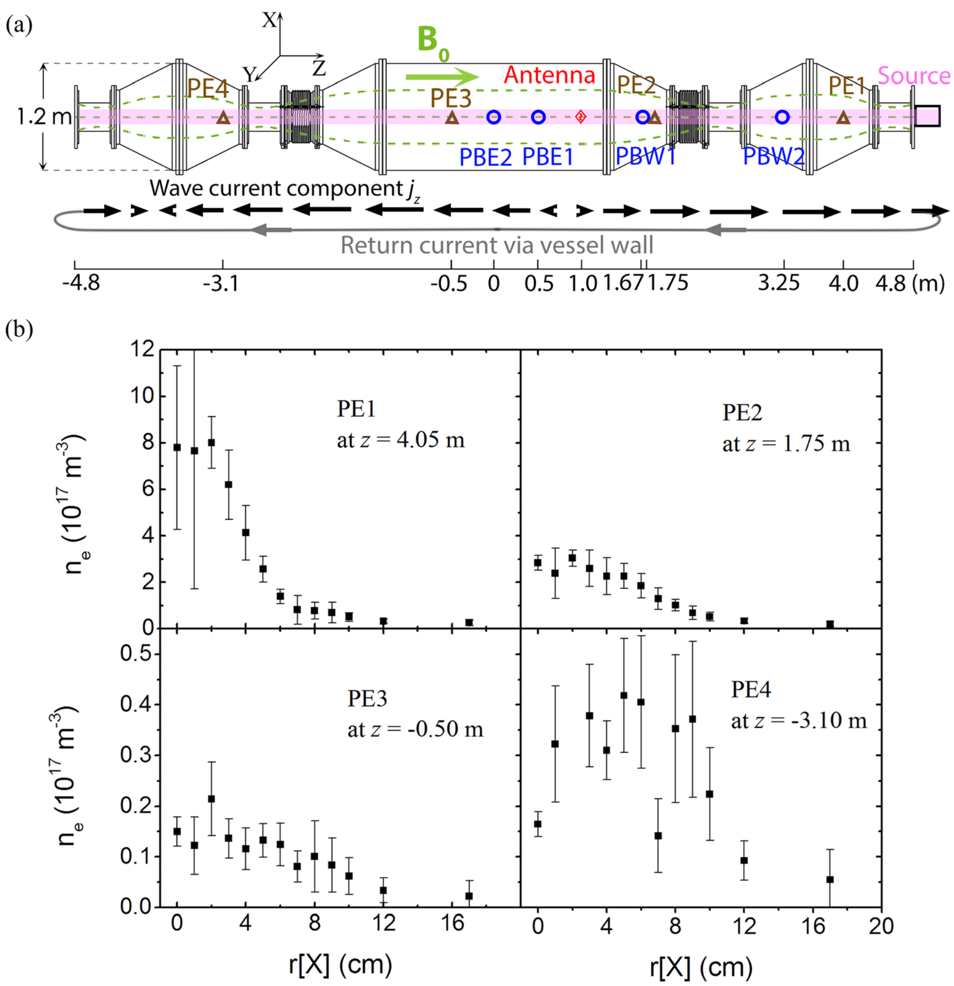

FIG. 1. (a) Machine diagram of the KMAX tandem mirror device. Hydrogen plasma is generated by a Nagoya type III antenna located at $z = 5.05$ m. The green dashed lines indicate the DC magnetic field lines towards $+z$; the brown triangles indicate the positions of triple probes PE1-4 from right to left; the blue circles indicate the magnetic probes PBE1, PBE2, PBW1, and PBW2 at $z = 0.00$ m, 0.50 m, 1.67 m, and 3.25 m; and the red diamond indicates the Alfvén launching antenna at $r = 0.05$ m. The black arrows at the bottom illustrate the axial current of the wave inside plasma at one moment, and the grey arrows indicate the return current possibly through endplates and vessel wall. (b) Radial density profiles at $z = 4.05$ m, 1.75 m, -0.50 m, and -3.10 m, measured by PE1-4, respectively.

constrains are presented in Figs. 2 and 3, respectively. Clearly, the pump fluctuation at $f = 368$ kHz has driven two daughter waves at $f_1 = 311$ kHz and $f_2 = 57$ kHz. Figure 2(a) displays the spectrum of output current from the oscillator whose Q is 35 000, high enough to be considered as a monochromatic emitter. Figures 2(b)–2(d) show the measured magnetic fluctuation spectra in the x, y, and z directions, respectively, and Fig. 2(e) shows the spectrum of ion saturation current collected by a single probe, i.e., one tungsten tip, integrated within magnetic probe suite PBW1. The launched fluctuation has been detected largely in the x direction, with an amplitude of ~0.12 gauss or ~0.04% of background field strength, which is in the same direction with the oscillating magnetic fields generated by this solenoidal antenna. Rather than launching a wave with a defined wavenumber and direction, this antenna more likely just perturbs the plasma or enhances the thermal fluctuations which are in phase with the driving oscillations. Hence, the wave may not be a single mode. In the low frequency limit, the degeneracy of torsional Alfvén waves and compressional waves can produce linearly polarized waves. It may explain why the δB_x component dominates in our measurements. The perturbation should travel in both directions; however, only the $+z$ directional propagation is found in our phase shift measurements [see Fig. 3(a) for the data]. Considering that the endplates of our device are conductors and the length of the wave is comparable with the device, the axial current of the wave can exit the plasma from one plate and re-enter from the other end in order to close its current loop in both parallel and perpendicular directions. In other words, the periodical boundary condition in our experiment allows the traveling wave to exist.

The most prominent feature of Fig. 2 is the presence of f_1 and f_2 on the z directional magnetic probe and electric probe. Those two waves only appear when both of the source oscillator and the helicon plasma are turned on. Different from the SAF discussed above, the magnetosonic wave must be accompanied by δB_z and density

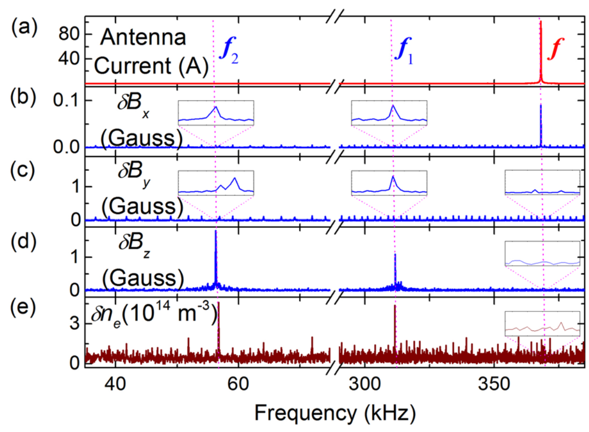

FIG. 2. Frequency spectrum of the Alfvén antenna current, magnetic field, and density fluctuation: (a) the Alfvén antenna emits waves at f=368 kHz; (b) the δB_x spectrum shows a peak at 368 kHz and also two small but distinguishable peaks at $f_1 = 311$ kHz and $f_2 = 57$ kHz, which can be clearly seen on the two inset panels; (c) the δB_y spectrum shows a small peak at f_1 but a negligible or questionable peak at f_2 and no discernible peak at 368 kHz; (d) the δB_z spectrum shows clearly the spontaneously decayed daughter waves resonating at 57 and 311 kHz and no peak at 368 kHz; and (e) the spectrum of plasma density fluctuation shows two peaks at 57 and 311 kHz.

fluctuations for its compression nature, as observed in our experiment [see Figs. 2(d) and 2(e)]. The δB_z components are 1.0–2.0 gauss in strength and ~0.3%–0.7% of the background field.[31]

B. Momentum conservation

In addition to energy conservation, the momentum must be conserved too, i.e., $k = k_1 + k_2$, which can be derived from the phase difference between magnetic probes. Figures 3(a) and 3(b) show their phase measurements in parallel and perpendicular directions, respectively, and the calculated $k_{\parallel 1} = 1.15 \pm 0.15$ rad/m and $k_{\parallel 2} = -0.30 \pm 0.10$ rad/m. The non-zero $k_{\parallel 1,2}$ of these compressive magnetic modes (δB_z) dictates the existence of non-zero perturbations in the perpendicular direction. This is consistent with the observation of the very modest δB_x and/or δB_y fluctuations at f_1 and f_2 in Figs. 2(b) and 2(c).

Figure 3(c) shows the parallelogram in the (ω, $k_\parallel$) plane reflecting the resonant conditions for parametric decay. Here, we denote the "+" sign to the wave propagating along the background field line direction, i.e., $+z$. This fluctuation propagating in the $+z$ direction has a phase velocity $(4.1 \pm 0.4) \times 10^6$ m/s, within the error of the predicted value $(5.0 \pm 1.3) \times 10^6$ m/s from the SAW dispersion considering the Hall MHD effect, $\omega = k_\parallel V_A \sqrt{1 - \omega^2/\Omega_{ci}^2}$, where V_A is the Alfvén speed.

Clearly, the mother fluctuation ($f = 368$ kHz, $k_\parallel = 0.55 \pm 0.05$ rad/m, and $k_\perp = 0 \pm 2$ rad/m) has decayed into a forward propagating wave ($f_1 = 311$ kHz, $k_{\parallel 1} = 1.15 \pm 0.15$ rad/m, and $k_{\perp 1} = -12 \pm 4$ rad/m) and a backward propagating wave ($f_2 = 57$ kHz, $k_{\parallel 2} = -0.30 \pm 0.10$ rad/m, and $k_{\perp 2} = 10 \pm 2$ rad/m), satisfying both energy and momentum conservation equations. Note that there have been extensive theoretical and simulation works on the parametric decay of SAWs into Alfvén and ion sound waves to explain the coronal heating, and our results have verified that there exists a channel for Alfvén fluctuations to decay into fast and slow waves. Moreover, it also shows that the parametric decay can produce the backward magnetic wave, a key ingredient for the turbulent cascade. Although not shown here, the measured amplitudes of waves are found to decrease with the radius, only ~0.1 G near the edge.

C. Identification of wave modes

1. Dispersion relation

A two-fluid description of low frequency magnetic waves is given by Ref. 5

$$\left[\omega^2(1 + k^2\delta_e^2) - V_A^2 k_\parallel^2\right] \cdot \left[\omega^2(1 + k^2\delta_e^2)(\omega^2 - C_s^2k^2) - V_A^2k^2(\omega^2 - C_s^2k_\parallel^2)\right] = \omega^2 V_A^4 k^2 k_\parallel^2(\omega^2 - C_s^2k^2)/\Omega_{ci}^2, \quad (1)$$

where C_S is the sound speed and δ_e is the electron inertial length. The first term describes the Alfvén and the second term magnetosonic waves. By substituting the experimental values of $C_S = 3.0 \times 10^4$ m/s, $V_A = 2.5 \times 10^6$ m/s, and $\delta_e = 0.04$ m in Eq. (1), we plot the relationship between ω and $k_\parallel$ for different $|k_\perp|$ in Fig. 3(d) as color-coded lines, along with the measured data of f_1 and f_2 waves as squares. Comparing with the model prediction, it is found the f_1 wave fits much better than the f_2 wave because $k_\perp$ is very sensitive to $k_\parallel$ in the low frequency regime.

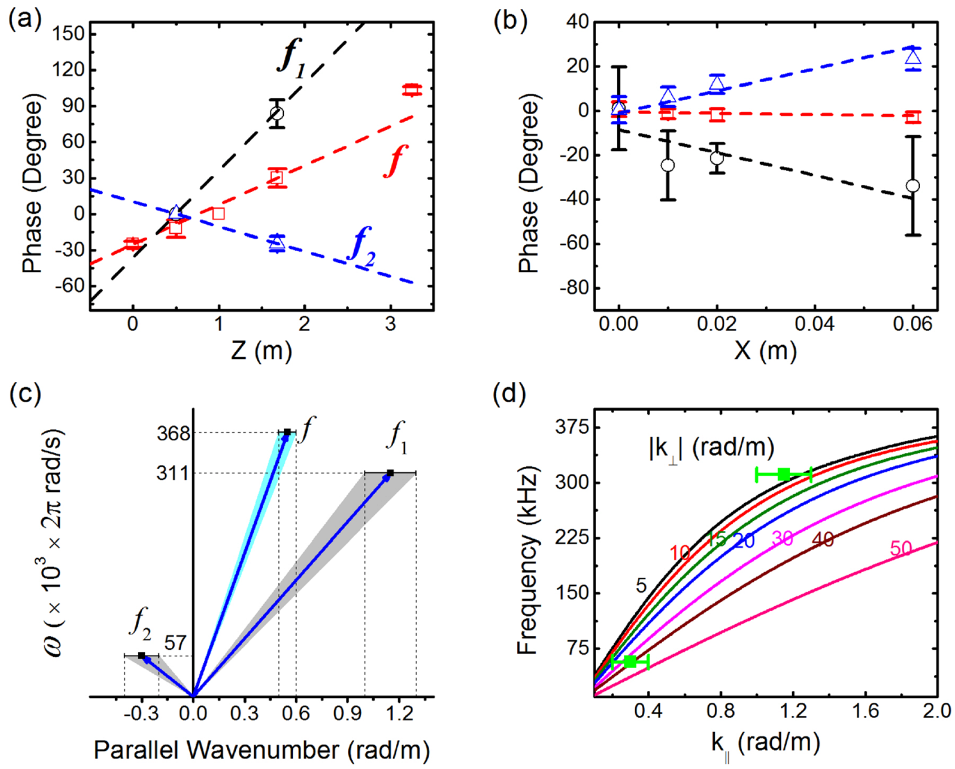

FIG. 3. (a) The phase shift relative to the antenna or PBE1, measured by four magnetic probes at different z's, with the red square, black circle, and blue triangle for waves f, f_1, and f_2, respectively. (b) The perpendicular phase shift versus x, and the symbols are used in the same manner as (a). (c) Parallelogram in the (ω, $k_{\parallel}$) plane reflecting the resonant conditions for parametric decay. The shaded error bars indicate the uncertainty in $k_{\parallel}$. (d) Theoretical prediction for different $|k_{\perp}|$, and measured data, f_1 and f_2, are indicated as squares.

2. Correlation between δn_e and δB_z

To further identify specific modes of these magnetosonic waves, we adopt the common approach used in space plasma. The correlation between density and parallel magnetic fluctuation is positive for the fast mode and negative for the slow mode.[32] In other words, δn_e and δB_z are in phase for fast magnetosonic waves and out of phase for slow magnetosonic waves.[5]

We can obtain the phase difference between δn_e and δB_z from the normalized Cross-Spectral Density (CSD) of measured δI_{sat} and daughter waves' δB_z, $\alpha = \mathrm{CSD}(\delta I_{sat}, \delta B_z)/\sqrt{\mathrm{PSD}(\delta I_{sat}) \cdot \mathrm{PSD}(\delta B_z)}$, where PSD stands for the Power Spectral Density. The result is shown in Fig. 4, where the red dotted line represents the degree of coherence $|\alpha|^2$ and the blue solid line represents the phase difference, $\arctan(\alpha)$. To have a more accurate estimation, we average the phase difference over a small frequency range whose coherence value is larger than 0.85, as shown in the grey region in Fig. 4, and the results are $35^\circ \pm 4^\circ$ for the f_1 wave and $150^\circ \pm 6^\circ$ for the f_2 wave. Adding the additional phase shift due to the radial separation of magnetic and electric probes, $-(16^\circ \pm 8^\circ)$ for f_1 and $+(12^\circ \pm 6^\circ)$ for f_2, the phase differences are found to be $19^\circ \pm 14^\circ$ for f_1 (311 kHz) and $162^\circ \pm 28^\circ$ for f_2 (57 kHz), respectively. The errors estimated above have included the errors due to the electron temperature fluctuation. Thus, it is reasonable to conclude that f_1 (in phase) is the fast and f_2 (out of phase) is the slow magnetosonic wave.

IV. ENERGY TRANSFERRING PROCESS

The energy transferring process is studied by analyzing the wave amplitudes as a function of time. Figure 5 shows that the SAF starts to grow at $t \sim 50$ μs, while two daughter waves are not present until $t \sim 200$ μs. This time delay reflects that a minimum strength of the pump wave is required to generate the other two waves.[33–35] A direct evidence of the energy transferring from the SAF to two daughter waves is shown as the dashed green line in Fig. 5(b), the SAF amplitude normalized to antenna current, which shows a relatively flat regime between $t = 50$ μs and $t = 200$ μs and starts to drop when two daughter waves appear.

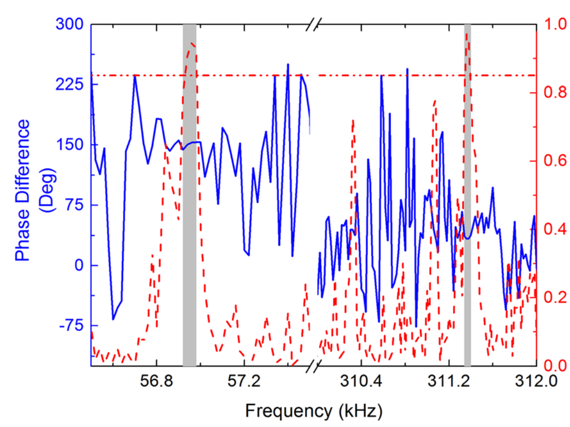

FIG. 4. Phase difference between δn_e and δB_z fluctuation. The cross-spectral density is plotted as blue solid line, while the corresponding coherence is shown as the red dotted line. The grey shades indicate the credible regions, where the coherence value must be greater than 0.85, for averaging the phase difference: $35^\circ \pm 4^\circ$ for wave f_1 and $150^\circ \pm 6^\circ$ for wave f_2.

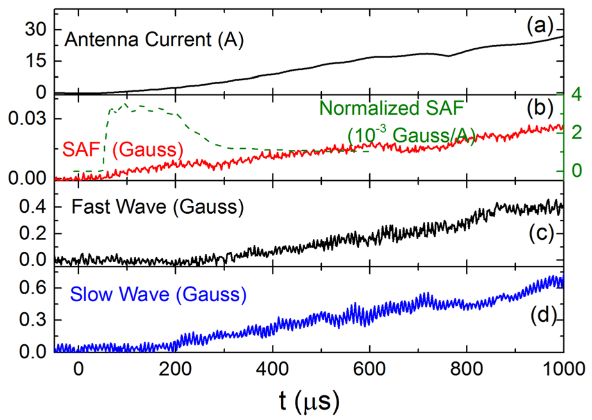

FIG. 5. Time history of (a) antenna current, (b) SAF and normalized SAF, (c) fast wave, and (d) slow wave amplitude from $t = 0$ to 1000 μs. The SAF amplitude normalized by antenna current, plotted as a green dashed line in panel (b), decreases at $t = 200$ μs, which indicates that SAF energy is being injected into the daughter modes.

V. CONCLUSION

A possible explanation for parametric decay to occur in this experiment is through the ponderomotive force.[35] The SAF and magnetosonic wave, or just thermal fluctuations in the initial stage, can couple together through the nonlinear force $\langle \delta j_y \cdot \delta B_z \rangle$, where δj_y and δB_z are the polarization current of the SAF and parallel magnetic field component of one daughter wave. Then, the force could influence or enhance the plasma velocity component δv_x of differential frequency corresponding to another daughter wave, which leads to density compression and rarefaction via term $k_\perp \cdot \delta v_x$. If the dispersion relations of these waves are satisfied by the experimental plasma parameters, two daughter waves could be fed continuously by pump waves and grow to an appreciable level.

In summary, we have presented experimental demonstration that a shear Alfvén fluctuation can spontaneously decay into a co-propagating fast magnetosonic wave and a counter-propagating slow magnetosonic wave. The constraints of energy and momentum conservation are satisfied. The modes of daughter waves are validated by comparison with a dispersion relation and by correlation between density and magnetic field fluctuation. Both of the daughter waves can be effectively damped, leading to the dissipation of wave energy. The slow magnetosonic wave has been widely deemed as a candidate for the heating of the coronal region. Similar to the observation of inward propagating waves in the coronal and chromosphere region, we also observed the counter-propagating wave in the experiment. Whether it may lead to the turbulent heating is a subject to the future study because the current source power is not high enough to see this effect. In a word, the experiment reported in this paper has opened a new window to study space plasma relevant physics, and it may also help to utilize Alfvén wave as an efficient supplementary heating method via the parametric decay process.

ACKNOWLEDGMENTS

This work was supported by the National Key R&D Program of China under Contract Nos. 2017YFE0301802 and 2017YFA0402500, the National Natural Science Foundation of China under Grant No. 11475172, and the Key Research Program of Frontier Sciences, CAS under Grant No. QYZDJ-SSW-DQC010.

REFERENCES

[1] M. E. Koepke, Rev. Geophys. **46**, RG3001, https://doi.org/10.1029/2005RG000168 (2008).
[2] E. M. Tejero, C. Crabtree, D. D. Blackwell, W. E. Amatucci, M. Mithaiwala, G. Ganguli, and L. Rudakov, Phys. Plasmas **22**, 091503 (2015).
[3] M. Yamada, R. Kulsrud, and H. Ji, Rev. Mod. Phys. **82**, 603 (2010).
[4] H. Ji, M. Burin, E. Schartman, and J. Goodman, Nature **444**, 343 (2006).
[5] N. F. Cramer, *The Physics of Alfvén Waves* (Wiley, 2011).
[6] W. Gekelman, S. Vincena, B. Van Compernolle, G. J. Morales, J. E. Maggs, P. Pribyl, and T. A. Carter, Phys. Plasmas **18**, 055501 (2011).
[7] S. Houshmandyar and E. E. Scime, Phys. Plasmas **18**, 112111 (2011).
[8] D. Leneman, W. Gekelman, and J. Maggs, Phys. Rev. Lett. **82**, 2673 (1999).
[9] C. Watts and J. Hanna, Phys. Plasmas **11**, 1358 (2004).
[10] R. Erdelyi and I. Ballai, Astron. Nachr. **328**, 726 (2007).
[11] R. Z. Sagdeev and A. A. Galeev, *Lectures on the Non-Linear Theory of Plasma* (W.A. Benjamin, New York, 1969).
[12] L. Del Zanna, M. Velli, and P. Londrillo, Astron. Astrophys. **367**, 705 (2001).
[13] S. S. Moiseev, V. N. Oraevsky, and V. G. Pungin, *Non-Linear Instabilities in Plasmas and Hydrodynamics* (Taylor & Francis, 1999).
[14] R. H. Kraichnan, Phys. Fluids **8**, 1385 (1965).
[15] P. Goldreich and S. Sridhar, Astrophys. J. **438**, 763 (1995).
[16] S. Sridhar and P. Goldreich, Astrophys. J. **432**, 612 (1994).
[17] X. Gao, Q. Lu, X. Li, Y. Hao, X. Tao, and S. Wang, Astrophys. J. **780**, 56 (2013).
[18] X. Gao, Q. Lu, X. Li, L. Shan, and S. Wang, Phys. Plasmas **20**, 072902 (2013).
[19] G. G. Howes, D. J. Drake, K. D. Nielson, T. A. Carter, C. A. Kletzing, and F. Skiff, Phys. Rev. Lett. **109**, 255001 (2012).
[20] S. Dorfman and T. A. Carter, Phys. Rev. Lett. **110**, 195001 (2013).
[21] S. Dorfman and T. A. Carter, Phys. Rev. Lett. **116**, 195002 (2016).
[22] V. N. Oraevsky, Nucl. Fusion **4**, 263 (1964).
[23] K. S. Karplyuk and V. N. Oraevskii, JETP Lett. **5**, 365 (1967).
[24] F. F. Cap, *Handbook on Plasma Instabilities* (Academic Press, 1982).
[25] G. Brodin and L. Stenflo, J. Plasma Phys. **39**, 277 (1988).
[26] S. Boldyrev, Phys. Rev. Lett. **96**, 115002 (2006).
[27] R. J. Morton, S. Tomczyk, and R. Pinto, Nat. Commun. **6**, 7813 (2015).
[28] Z. X. Liu, J. S. He, and L. M. Yan, Res. Astron. Astrophys. **14**, 299 (2014).
[29] Q. Zhang, P. Shi, M. Liu, M. Lin, and X. Sun, Fusion Sci. Technol. **68**, 50 (2015).
[30] J. L. Kline, E. E. Scime, P. A. Keiter, M. M. Balkey, and R. F. Boivin, Phys. Plasmas **6**, 4767 (1999).
[31] L. Matteini, S. Landi, L. Del Zanna, M. Velli, and P. Hellinger, Geophys. Res. Lett. **37**, L20101, https://doi.org/10.1029/2010GL044806 (2010).
[32] G. G. Howes, S. D. Bale, K. G. Klein, C. H. K. Chen, C. S. Salem, and J. M. TenBarge, Astrophys. J. Lett. **753**, L19 (2012).
[33] C. S. Liu and V. K. Tripathi, Phys. Rep. **130**, 143 (1986).
[34] J. L. Kline and E. E. Scime, Phys. Plasmas **10**, 135 (2003).
[35] F. F. Chen, *Introduction to Plasma Physics and Controlled Fusion* (Springer, 2006).